An Empirical Investigation of Bow-Force Limits in the Schelleng Diagram

Erwin Schoonderwaldt[1], Knut Guettler[2], Anders Askenfelt[1]

[1] KTH-Computer Science and Communication, Dept. of Speech, Music and Hearing, Lindstedtsvägen 24,
100 44 Stockholm, Sweden. schoondw@kth.se; andersa@speech.kth.se

[2] Norwegian Academy of Music, P.B. 5190 Majorstua, 0302 Oslo, Norway. knut.guettler@nmh.no

Summary

An experimental study of the upper and lower bow-force limits for bowed violin strings is reported. A bowing machine was used to perform bow strokes with a real violin bow on steel D and E strings mounted on a rigid monochord and on a violin. Measurements were systematically performed for 11 values of relative bow-bridge distance and 24 values of bow force at four bow velocities (5, 10, 15 and 20 cm/s). The measured string velocity signals were used to compile Schelleng diagrams, showing the distribution of different classes of string motion (multiple slipping, Helmholtz motion, raucous motion). It was found that the maximum bow-force limit for Helmholtz motion corresponded well to Schelleng's equation in modified form, taking the shape of the (hyperbolic) friction curve into account. The minimum bow force was found to be independent of bow velocity, which is in clear contradiction to Schelleng's prediction. Observations and simulations suggested that the breakdown of Helmholtz motion at low bow forces involves a mechanism related to ripple and corner rounding which was not taken into account in Schelleng's derivation of minimum bow force. The influence of damping showed only qualitative agreement with Schelleng's predictions.

PACS no. 43.75.De

1. Introduction

Tone production in a bowed-string instrument is governed by a complex frictional interaction between the bow and the string. The physics of the interaction provides the player the means to control the sound via the three main bowing parameters bow velocity, bow force and bow-bridge distance, but imposes constraints as well.

In classical playing Helmholtz motion is the established norm for violin sound, corresponding to a regular string vibration with one slip and stick phase per fundamental period. Two requirements on the bow force must be met to maintain Helmholtz motion: (1) during the stick phase the bow force must be high enough to avoid premature slipping of the string, and (2) the bow force must be low enough that the circulating Helmholtz corner can trigger the release of the string at the initiation of the slip phase. For a given combination of bow velocity and bow-bridge distance there is a certain range in bow force which must be respected.

1.1. Bow-force limits

The limits of the playable region have been formalized by Schelleng [1], who gave expressions for the minimum and

the maximum bow force as function of relative bow-bridge distance β and bow velocity v_B:

$$F_{max} = \frac{2Z_0 v_B}{(\mu_s - \mu_d)\beta},$$ (1)

and
$$F_{min} = \frac{Z_0^2 v_B}{2R(\mu_s - \mu_d)\beta^2}.$$ (2)

Here Z_0 is the characteristic transverse impedance of the string, μ_s the maximum static friction coefficient, and μ_d the dynamic friction coefficient. R originates from Raman's string model on which Schelleng based his derivations with a fixed string termination at the nut and a pure mechanical resistance R at the bridge. The friction coefficient delta $(\mu_s - \mu_d)$ will be referred to as $\Delta\mu$ in the following.

It could be noted that the factor 2 in the numerator of equation (1) was not present in the original equation derived by Schelleng, but was mentioned by him in a footnote (footnote #10 in [1]). This factor is a necessary condition for complete reflection of the discontinuity arriving from the nut at the bow, and previous studies of the maximum bow-force limit have taken this factor into account, e.g., Askenfelt [2], Woodhouse [3], Schumacher [4], and Galluzzo [5].

Schelleng introduced a diagram with a log-log representation of relative bow force versus relative bow-bridge distance. In the classical Schelleng diagram the upper and

lower bow-force limits form straight lines with slopes of -1 and -2, respectively, demarcating a triangular-shaped playable region with Helmholtz motion. An important underlying assumption is that the friction coefficient delta $\Delta\mu$ is constant. This is mostly a reasonable approximation for high bow velocities and short bow-bridge distances, but it does not hold in general since the dynamic friction coefficient is dependent on slip velocity. This was already realized by Raman [6] and used by him to explain his observation that the minimum bow force approached a finite minimum for decreasing bow velocities.

The variation in $\Delta\mu$ can be accounted for in the Schelleng equations by introducing a functional form of the friction curve. This was done by Schelleng for the minimum bow force using a hyperbolic friction curve of the form:

$$\mu = \mu'_d + K/(z - z_0), \tag{3}$$

in which z is the relative slip velocity v_B/β, z_0 a velocity offset to obtain a finite value for μ_s at $z = 0$, μ'_d the asymptotic value of μ for $z \to \infty$, and K a constant determining the curvature. The friction coefficient delta can then be rewritten as:

$$(\mu_s - \mu_d) = z(\mu_s - \mu'_d)/(z + z_0)$$

and the modified minimum bow force is then obtained by substitution of $(\mu_s - \mu_d)$ in equation (2):

$$F_{min} = \frac{Z_0^2}{2R(\mu_s - \mu'_d)} \cdot \frac{v_B + \beta z_0}{\beta^2}. \tag{4}$$

Note that equation (4) reduces to equation (2) when $z_0 = 0$. The factor $(\mu_s - \mu'_d)$ is a constant, representing the difference between the maximum static friction coefficient and the asymptotic value of μ (the minimum value in case of the hyperbolic friction curve). It will be referred to as $\Delta\mu'$ in the following.

In the modified model the minimum bow force approaches a finite minimum when the bow velocity approaches zero, but the shape of the lower bow-force limit in the Schelleng diagram is also altered. When v_B approaches zero, the minimum bow force becomes proportional to $1/\beta$, rather than $1/\beta^2$. Furthermore, for constant v_B the term βz_0 in equation (4) gains relative importance with increasing β, leading to a curvature in the lower bow-force limit.

Also the maximum bow force can be modified, taking the functional form of the friction curve into account. Using the same hyperbolic friction curve (equation 3) an analogue derivation of the maximum bow force yields

$$F_{max} = \frac{2Z_0}{(\mu_s - \mu'_d)} \cdot \frac{v_B + \beta z_0}{\beta}. \tag{5}$$

The consequences for the upper bow-force limit are the same as for the lower limit. The maximum bow force approaches a finite minimum when v_B approaches zero, and the upper bow-force limit in the Schelleng diagram will be slightly curved.

This way of rewriting the Schelleng bow-force limits is based on the assumption that the friction curve can be described by a hyperbolic function, only dependent on the relative velocity. This type of friction curve has been applied in many bowed-string simulations. It is also possible to derive modified Schelleng equations for a more general class of velocity-dependent friction curves, as Schumacher [4] has done for the maximum bow force.

Another approximation used by Schelleng was to neglect the effects of torsion and dispersion in the string. However, the rotational compliance of the string can have a significant influence on the maximum bow force. In order to take this into account the transverse characteristic impedance Z_0 in equations (1) and (5) should be replaced by the combined characteristic tangential impedance $Z_{tot} = Z_0 Z_R/(Z_0 + Z_R)$, with Z_R the torsional wave impedance, which is typically a factor 2 to 4 higher than Z_0 [4, 7]. This results in a lowering of the maximum bow force. In the expressions for minimum bow force, equations (2) and (4) the factor Z_0^2 should be replaced by $Z_{tot} Z_0$, as the factor Z_0/R is associated with the transfer function from string to body and is not influenced by torsion of the string at the bow-string contact point.

1.2. Previous measurements of bow-force limits

Only a few experimental studies of bow-force limits have been published, most of them focusing on the minimum bow force. The earliest known experimental study of minimum bow force was done by Raman [6], using an ingenious mechanical bowing machine, a real bow and a real violin. His main findings were that (1) the minimum bow force was proportional to $1/\beta^2$, (2) the minimum bow force increased with bow velocity (however generally not proportionally), and (3) the minimum bow force was strongly increased at certain resonances of the violin. The first two findings were later confirmed by measurements of Lazarus (see Cremer [8], section 4.5).

The maximum bow force has been experimentally measured by Schumacher [4] for a number of different strings. A real bow and violin were used, and bow velocity and bow force were controlled by a computer-controlled bowing machine. From the measurements the values of $\Delta\mu$ and $\Delta\mu'$ were estimated (in Schumacher's [4] notation indicated by $\Delta\mu^*$ and $\Delta\mu$, respectively), using Schelleng's equation for maximum bow force in a generalized form and taking the torsional wave impedance of the string into account. The findings suggested a reasonable agreement between the observed values of maximum bow force and Schelleng's generalized equation.

Previous experimental verifications of a complete Schelleng diagram under well-controlled conditions have been limited to a cello string at a single bow velocity [5]. In that experiment a computer-controlled bowing machine was used to bow a cello D string with a rosined perspex rod at a velocity of 5 cm/s. The rod was considered as a rigid point bow, and was chosen to allow for an easier comparison of the experimental results with bowed-string simulations. Also in this study, the dependence of the observed

bow force limits on bow-bridge distance was found to be in reasonable agreement with Schelleng's equations (equations 1 and 2). At some particular values of β, close to integer ratios, also S-motion was found, characterized by very large ripple. S-motion occurred mostly beyond the maximum bow force limit, but also at higher bow forces within the Helmholtz region, forming 'columns' in the Schelleng diagram. S-motion can be considered as a 'higher' type of string motion, described in detail by Lawergren [9].

1.3. Influence of the instrument, corner rounding and ripple

The minimum bow force is dependent on the energy losses. In Schelleng's equation for the minimum bow force (equations 2 and 4) this is expressed by the mechanical resistance R, which represents the combined losses due to the internal friction in the string, the reflections at both string terminations (bridge and nut/finger) and the bow-string interaction. As the bridge mobility is strongly dependent on frequency due to the resonance structure of the instrument, the minimum bow force can vary greatly between notes played on the same instrument or between different instruments. For this reason the minimum bow force and its variation within a single instrument has often been considered as a promising measure of the 'playability' of an instrument [10]. Playability has been introduced as a concept reflecting how an instrument reacts to the actions of the player. This aspect was taken up already by Raman [6] in his measurements of minimum bow force for different notes. Saunders [11], using a rotating group of thin celluloid disks to bow the violin under controlled conditions, carried the work further by exploring the minimum bow force necessary to 'make the violin speak properly' for different notes, and made comparisons with 'loudness curves' showing the acoustical output for bowed notes at different pitches.

It is well known that the Raman string model is not very realistic. The approximation that the string termination at the bridge is purely resistive implies that the reflection function is characterized by a delta function. This means that the shape of the reflected waves remains unaltered, the reflections only being attenuated by a constant factor depending on the amount of damping. As a result the Raman model does not account for corner rounding and ripple, typically present in observations of real string vibrations and in realistic bowed-string simulations.

Woodhouse [3] has derived a more general equation for the minimum bow force, without the restrictive assumption of the Raman model. This equation allowed him to use measured admittance curves to predict the frequency dependence of the minimum bow force for particular instruments. The generalization also makes it possible to derive the minimum bow force for other theoretical instrument models. This feature was demonstrated by Woodhouse [3] for the Cremer model, which is similar to the Raman model, but with an additional reactive component (see Cremer [8] and Woodhouse [10]). It was shown that the minimum bow force for Cremer's model, and for models characterized by narrow reflection functions in general,

was very low. Simulations showed that the slip phase at low bow forces could be significantly prolonged due to corner rounding, even to an unrealistic extent. The discrepancy between these simulations and a real bowed string was explained by the presence of another source of perturbing force during the stick phase, namely 'secondary' waves or ripple, the reflected waves between the bow and the bridge during the stick phase. This effect is also ignored in Schelleng's arguments for the presence of a minimum bow force.

The lengthening of the slip phase by corner rounding can be easily understood as follows. In a crude approximation corner rounding can be described by a moving-average filter of finite width. With repeated filtering the Helmholtz corner becomes increasingly rounded, an effect counteracted by resharpening at the bowing point. Corner sharpening increases with bow force and friction delta. As an effect of corner rounding the sudden transition from stick to slip is smeared out in time, resulting in a flank with finite slope, a longer duration of the slip phase and a shorter duration of the slipping part with nominal slip velocity. (The duration of the slip at half height remains unchanged, corresponding to the nominal slip duration of ideal Helmholtz motion). When the effect of rounding extends over a time interval longer than the nominal duration of the slip phase, the nominal slip velocity is no longer reached, and the slip phase starts to collapse.

Even though this simplified representation of corner rounding is far from realistic the qualitative influence on the shape of the slip phase is described rather well, comparable with more sophisticated models of corner rounding (see for example the Appendix in Boutillon [12]) and measured string-velocity signals.

1.4. Aim of the study

The main purpose of the current study was to perform a systematic experimental investigation of the bow-force limits in the Schelleng diagram. In order to stay close to the reality experienced by the player a normal violin bow was used to bow standard strings mounted on a monochord and on a violin. Empirical Schelleng diagrams were compiled for different strings and at different bow velocities. The bowing parameters were controlled with a computer-controlled bowing machine, and an interactive, semi-automatic method was used for string motion classification (see section 2). The observed bow-force limits were used for evaluation of Schelleng's equations by means of curve fitting and estimation of the friction-coefficient delta (section 3).

A second experiment was performed to shed more light on the string motion close to the minimum bow force (section 4). In this experiment the minimum bow force was determined more accurately, taking the variance observed in this region into account. Also the transition from Helmholtz motion to multiple slipping was studied more closely in relation to the shape of the slip phase.

In a third experiment, the influence of the damping factor R on the minimum bow force was investigated (section 5). For this purpose the minimum bow force was measured

on a monochord and a violin using both open and stopped strings. The values of R were estimated from the decay times of the plucked notes, allowing for direct comparison with Schelleng's equation for minimum bow force.

In addition to a detailed investigation of the bow-force limits two other features which also are dependent on the combination of bowing parameters were studied in relation to the Schelleng diagram: pitch flattening and the spectral centroid. The analysis of these data will be reported elsewhere.

2. Method

2.1. Experimental setup

Empirical Schelleng diagrams were obtained using a normal bow driven by a computer-controlled bowing machine [13]. Most measurements were performed on a rigid monochord, in order to avoid the influence of the prominent body modes of a violin. The monochord consisted of a duraluminium bar with a U-shaped cross-section (60×40 mm), glued onto a solid piece of hardwood. The dimensions and geometry of the monochord were copied from a standard modern violin (string length 325 mm, bridge height 42 mm above a reference line through the nut and the tailpiece rest). The solid duraluminium bridge had the same shape as a normal violin bridge with notches for the strings. Also the nut, made of a hard plastic, was modeled according to a violin. At both string supports (bridge and nut) a piece of tape (medical waterproof tape, thickness 0.27 mm) was applied to improve the contact between the string and the support and add appropriate damping. Without tape it was observed that pizzicato notes sometimes resulted in sitar-like sounds, indicating the presence of a non-linear interaction between the string and the string termination. The violin used for some of the measurements in section 5 was a modern master violin built in 1997 by Matthieu Besseling.

The strings used were violin D and E steel strings manufactured by Prim ('Medium tone'). The D string had a steel core and a chrome steel winding (outer diameter 0.70 mm, linear density $\rho_L = 1.29$ g/m, $Z_0 = 0.25$ kg/s). The E string was a plain steel string (diameter 0.26 mm, $\rho_L = 0.41$ g/m, $Z_0 = 0.18$ kg/s). The strings were tuned to nominal pitch: D4 = 293 Hz and E5 = 660 Hz. The linear densities were carefully measured using the speaking lengths of the strings as samples after having been brought up to nominal playing frequency. The characteristic impedance was calculated as $Z_0 = 2\rho_L L f_1$, where L is the speaking length and f_1 fundamental frequency.

The bow used was a carbon fibre composite bow manufactured by Leopold, [1] with a total mass of 58 g. The width of the bow hair ribbon was 10 mm. The rosin used was Pirastro Oliv/Evah.

The transverse string velocity under the bow was measured using a small cylindrical magnet (diameter 6 mm). The gap between the magnet and the string was typically 1 mm. The magnet was mounted in a plastic holder

---

[1] http://www.leopold-bow.com

which could be accurately positioned in two directions by means of two adjustable slides. The induced voltage was picked up by electrodes attached to the passive parts of the string and amplified with a balanced microphone preamplifier (Symmetrix SX 202). The string velocity signal was recorded into the computer using an external sound device (Tascam US-122) at a sampling rate of 44.1 kHz.

A linear relation between the induced signal and the transverse string velocity requires that the width of the magnet is large compared to the vibration amplitude. Assuming ideal Helmholtz motion (and disregarding the static displacement), the amplitude of string displacement at the bowing point is estimated by $(1 - \beta) T_1 v_B$, where T_1 is the fundamental period. In the experiments the displacement amplitude during Helmholtz motion did not exceed 0.6 mm (for $v_B = 20$ mm/s, $\beta = 1/6$ and $T_1 = 3.4$ ms), which is a factor 10 less than the diameter of the magnet. Even in the case of other types of motion, such as raucous motion or anomalous low frequencies (ALF), which are characterized by prolonged periods normally up to three times T_1, the string displacement was considerably smaller than the width of the magnet.

Due to the finite width of the magnet the measured string velocity signal is somewhat smoothed. Assuming that the effective width of the magnetic field was 50% wider than the actual magnet diameter, the averaging window with respect to one fundamental period is about $d/2L \approx 0.01$. For the D string sampled at 44.1 kHz (150 samples/period) the averaging window is about 1.5 samples, which is negligible for the purpose of string motion classification.

2.2. The bowing machine

The bowing machine was a converted daisy wheel printer controlled by an AT computer [13]. The machine performed bow strokes defined in input files containing target bow position and bow force contours sampled at a rate of 600 Hz. The bowing machine could reliably produce bow velocities up to 30 cm/s (and probably higher). In the range 5-30 cm/s the maximum amplitude of the velocity fluctuations during steady-state bow strokes (with moderate bow-force) was of the order of 5 mm/s. The RMS value of the fluctuations at the lowest bow velocity (5 cm/s) reached about 5%.

The maximum bow force that could be supplied by the servo motor of the bowing machine was limited to about 2 N in the lower half of the bow, decreasing to about 1 N in the upper half. In order to reach higher bow forces an extra mass (327 gram) was mounted on the bow hold to increase the contribution of gravity to the torque. In this way bow forces up to 3 N could be reached when approaching the frog.

The maximum fluctuation in bow force during steady-state bow strokes was about 20 mN for down-bows and 30 mN for up-bows throughout the range of used bow forces (49-3000 mN). Thus, the relative fluctuation error was largest at low bow forces. The RMS value of the fluctuations relative to the lowest target force (49 mN) was

about 20% for down-bows and 30% for up-bows. The relative RMS value dropped below 10% for target forces higher than 100 mN for down-bows and 143 mN for up-bows.

2.3. Bowing parameters

The bowing parameters studied included the relative bow-bridge distance β, bow force F_B and bow velocity v_B. The parameter ranges were chosen to represent a substantial part of the control space in normal violin playing (see e.g. Askenfelt [2]).

The β range (about 1/30 to 1/6), was divided into a grid of 11 logarithmically-spaced values (11, 13, 15, 18, 21, 24, 29, 34, 39, 46 and 55 mm). The bow-bridge distance was set by placing the magnet under the string with its center in the target position. Then the alignment of the bowing machine was adjusted so that the middle of the bow hair ribbon coincided with the center of the magnet. The achieved positioning accuracy was estimated to be about ±0.5 mm. For all presented measurements the bow hair was flat on the string (no bow tilt). It could be noted that due to the finite width of the bow hair (10 mm) a substantial range of β values were covered across the contact surface with the string. For the shortest bow-bridge distance used (11 mm) the edges of the bow hair corresponded to β values of 1/54 and 1/20, respectively. For the six shortest bow-bridge distances (up to 24 mm), the bow positions were overlapping, meaning that the previous center-line position was covered by the bow hair ribbon in the next position.

The force range (49–3000 mN) was divided into a grid of 24 logarithmically-spaced values (49, 58, 70, 84, 100, 120, 143, 171, 205, 245, 293, 350, 419, 501, 599, 716, 857, 1025, 1226, 1466, 1753, 2097, 2508 and 3000 mN). The bow velocities used were 5, 10, 15 and 20 cm/s.

2.4. Bow strokes

In the design of the bow strokes the following criteria were taken into account: (1) Helmholtz motion should be developed in the initial phase of the bow strokes, and (2) the steady part of the bow strokes (with constant bow velocity and bow force) should last long enough to establish a stable string motion pattern. These criteria resulted in a standard shape for the bow velocity and bow force contours as shown in Figure 1. The bow strokes were divided into four time intervals, the initial phase T_{init}, the transition phase T_{trans}, the steady phase T_{steady} and the stop phase T_{stop}. The exact shape and the duration of the different phases were dependent on the target values of bow velocity and bow force, as well as on the conditions required for rapid development of Helmholtz motion. The total duration of the dynamic part ($T_{trans}+T_{steady}+T_{stop}$) of the bow stroke was constrained due to limited stroke of the bowing machine (max. 31 cm), which necessitated a trade-off between T_{trans} and T_{steady}, especially at higher bow velocities. Typical durations used were 0.5-1.0 seconds for T_{trans} and 0.65-4.0 s for T_{steady}.

For the two highest bow velocities (15 and 20 cm/s) T_{steady} was rather short. For comparison, Galluzzo [5] monitored the motion of a cello D string by taking a
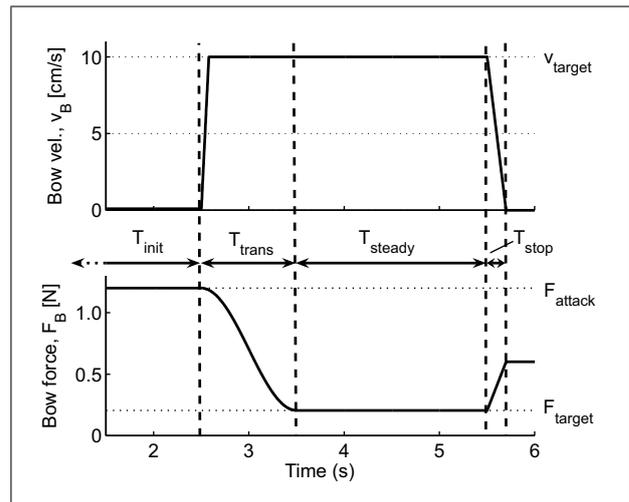
Figure 1. An example of bow velocity and bow force contours used for measuring Schelleng diagrams. The acceleration-force combination during the attacks (start of T_{trans}) was chosen to obtain short pre-Helmholtz transients. During the transition phase T_{trans} the force was smoothly changed to the target force F_{target}. Bow velocity and bow force were kept constant during T_{steady}.

100-ms sample after 2 s of steady bowing. However, the string velocity signals measured in the current experiments showed that changes in string motion occurred practically simultaneously with changes in bow forces (both upwards and downwards) and no long delays were observed for transitions between different types of string motion. Thus, it was concluded that T_{steady} was long enough for reliable string motion classification also at the two highest bow velocities.

2.5. Experimental conditions

External factors will influence the string motion to some extent. Such factors include tuning, amount and quality of the rosin, bow-hair tension, and possibly also temperature and humidity. On a longer term aging of the string and the bow hair could also play a role. Steps were taken to keep the experimental conditions as constant as possible. Before each measurement session the string was tuned to nominal frequency and a small amount of rosin was applied by rubbing the bow hair against the piece of rosin back and forth once or twice. The bow was then prepared for playing by drawing some long notes before the actual measurements started. Furthermore, the time span in which the measurements were performed was kept as short as possible. In order to minimize possible trends in data due to external factors the bow-bridge distances were measured in random order in most of the presented measurements.

2.6. String motion classification method

The compilation of Schelleng diagrams requires classification of different types of string motion. Examples of the most common types, including Helmholtz motion, multiple slipping and raucous motion are shown in Figure 2. Other, more peculiar string vibration patterns observed were anomalous low frequency (ALF) and S-motion.
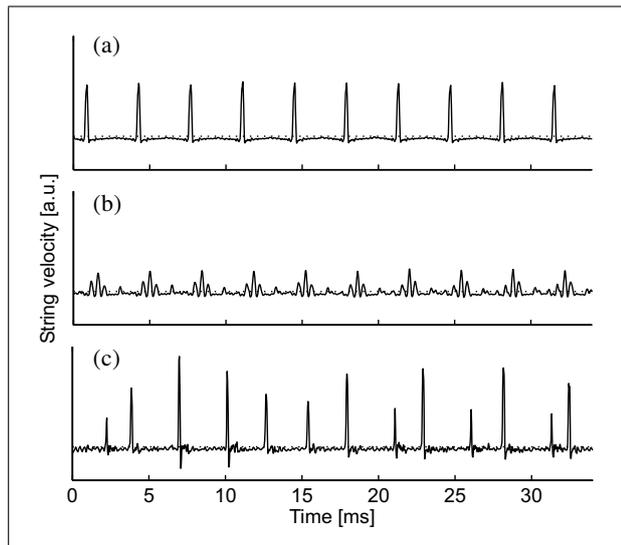
Figure 2. Examples of common types of string motion (velocity) as recorded in the experiments: (a) Helmholtz motion, (b) multiple slipping and (c) raucous motion.

Figure 3. Examples of string motion classification diagrams for (a) Helmholtz motion, (b) multiple slipping motion, (c) raucous motion, and (d) anomalous low frequency (ALF). The classification diagrams are scatter plots of displacement during the slip phase d_{slip} versus slip-to-slip interval T_{slip}. Each point in the diagram corresponds to one detected slip phase. The units in the diagram are normalized with respect to the fundamental period T_1 and displacement for ideal Helmholtz motion. The intersection between the two dashed lines indicates the reference point for Helmholtz motion.

In order to facilitate the classification of string velocity signals a novel interactive method was developed. First, the slip phases in a selected interval were identified, using a simple velocity threshold criterion. Second, two features were determined for each detected slip phase: (1) the slip-to-slip time interval (between the previous and the current slip phase), and (2) the string displacement during the slip phase. These features were then displayed in a two-dimensional scatter plot of displacement versus time, in the following referred to as a classification diagram. The velocity threshold for the detection of slip phases was by default $-v_B$, but could be manually adjusted. As the string velocity signals were not calibrated v_B was estimated by the median of the signal during stick phase. The onset and offset times of the detected slip phases were determined from the zero-crossings, using linear interpolation.

In case of ideal Helmholtz motion with constant v_B and β all slip phases coincide at one point in the classification diagram with the fundamental period T_1 as time coordinate and the extent of the string displacement at the bowing point $(1 - \beta)T_1 v_B$ as the displacement coordinate (Helmholtz reference point). All measured points were normalized with respect to this reference point.

The different types of string motion were in most cases clearly recognizable from the emerging pattern in the classification diagram. Some typical examples are shown in Figure 3a–d, illustrating the classification diagrams of the string motions in Figure 2. In case of Helmholtz motion (panel a) the points fall into a single cluster close to the reference point. In case of multiple slipping (panel b) the points form a set of two or more clusters, corresponding to the different slip phases within the fundamental period. This reflects the fact that multiple slipping is a rather persistent periodic type of motion. All clusters lie within the reference rectangle spanned up by the fundamental period and the displacement of ideal Helmholtz motion, but not

necessarily on the diagonal. In case of raucous motion (panel c) the points are more or less randomly distributed across the diagram, reflecting the aperiodicity of this type of motion. Some points fall outside the reference rectangle, indicating the presence of prolonged periods. Finally, in case of ALF (panel d) the points fall in a single cluster, indicating the periodicity of the signal. The cluster lies far outside the reference rectangle, on an extended diagonal between the origin and the reference point.

The described classification method has some similarities with the classification method of transverse bridge-force waveforms used by Woodhouse [14]. In that method a classification histogram is constructed, based on a selected portion of the bridge-force signal. The distances between the peaks in the histogram correspond to the magnitude of the flyback force, which is proportional to the string displacement during the slip phase measured close to the bridge. No explicit timing measurements were used by Woodhouse for the classification.

3. Experiment I: Empirical Schelleng diagrams

3.1. Experimental procedure and analysis

Empirical Schelleng diagrams were measured for the D string on the monochord at four bow velocities (5, 10, 15 and 20 cm/s), 11 values of β and 24 values of F_B. For each bow-bridge distance a series of bow strokes was per-
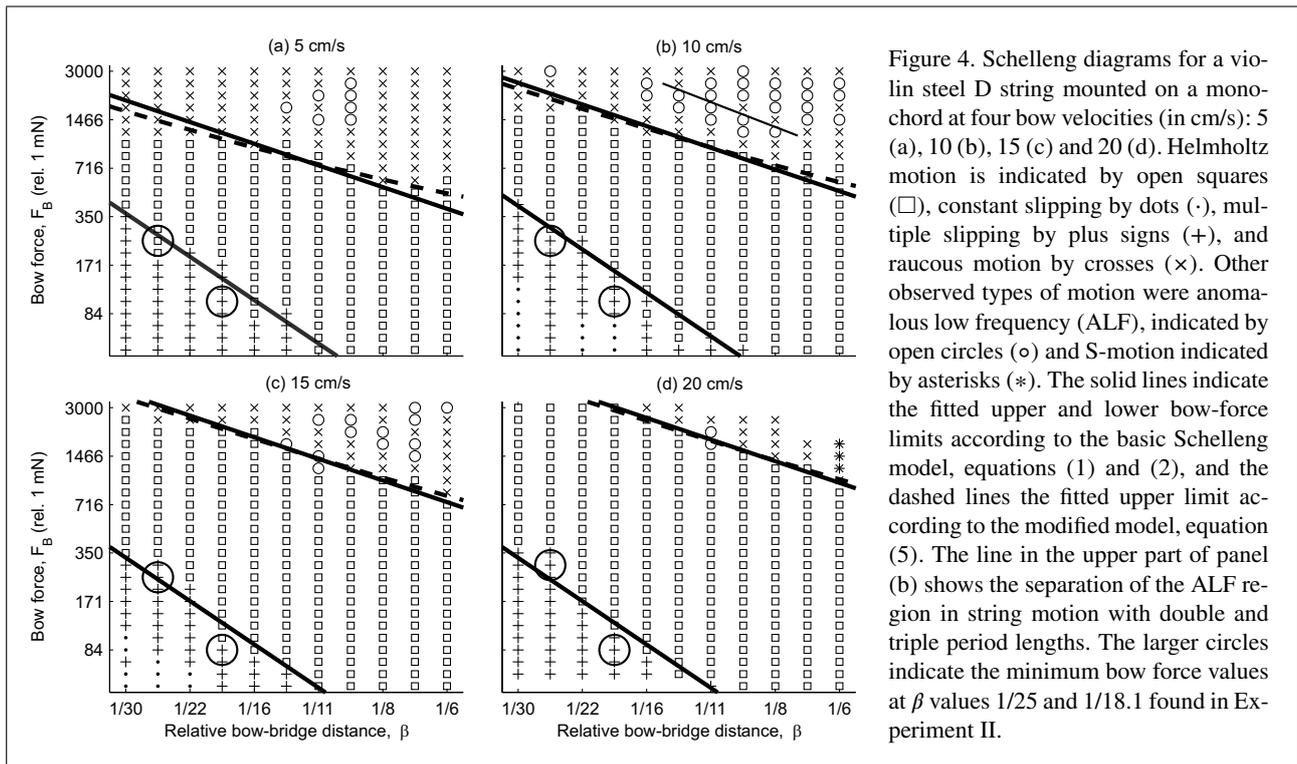
Figure 4. Schelleng diagrams for a violin steel D string mounted on a monochord at four bow velocities (in cm/s): 5 (a), 10 (b), 15 (c) and 20 (d). Helmholtz motion is indicated by open squares (□), constant slipping by dots (·), multiple slipping by plus signs (+), and raucous motion by crosses (×). Other observed types of motion were anomalous low frequency (ALF), indicated by open circles (○) and S-motion indicated by asterisks (∗). The solid lines indicate the fitted upper and lower bow-force limits according to the basic Schelleng model, equations (1) and (2), and the dashed lines the fitted upper limit according to the modified model, equation (5). The line in the upper part of panel (b) shows the separation of the ALF region in string motion with double and triple period lengths. The larger circles indicate the minimum bow force values at β values 1/25 and 1/18.1 found in Experiment II.

formed with successively higher bow force and three repeated measurements at each force value. String motion classification was applied on a manually selected portion of the signal (10 nominal periods), typically close to the end of the steady part of bowing. A final decision about the type of string motion was taken by the experimenter after inspection of both the string-velocity signal and the classification diagram.

3.2. Playable region and bow-force limits

The obtained Schelleng diagrams are displayed in Figure 4, in which the observed types of string motion are indicated with different symbols. At all bow velocities a continuous playable region of Helmholtz motion could be observed with clear upper and lower bow-force limits. The triangular shape of the Helmholtz regions is in agreement with Schelleng's observations [1]. The upper and lower bow-force limits formed approximately straight lines, in good agreement with the predictions of equations (1) and (2) (see section 3.3). Above the upper bow-force limit mostly raucous motion was observed, as well as some cases of anomalous low frequency (ALF) and S-motion. Below the lower limit multiple slipping, multiple flyback and constant slipping motion were observed.

The four panels in Figure 4 show how the playable region depended on bow velocity. It can be seen that the playable region became larger with increasing bow velocity. The upper bow-force limit was clearly shifted upward, while the lower limit remained rather constant. The observation that the upper bow-force limit increased with increasing bow velocity is in agreement with equation (1), which predicts that the upper limit is proportional to v_B.

However, the independence of the lower bow-force limit on bow velocity is a surprising result in view of that v_B also appears in the numerator of equation (2). This behavior will be further examined in sections 3.8 and 4.3.

An interesting detail was that clear playable regions of anomalous low frequencies (ALF) were found, especially at bow velocities of 10 and 15 cm/s (see Figure 4b and c). Different types of ALF were found, mostly with periods of twice or three times the fundamental period. The latter was found at higher bow forces and larger values of β. In Figure 4 (b) the separation between the ALF regions with twice and three times the fundamental period is indicated. The shape of the ALF regions resembles the triangular region of Helmholtz motion, showing decreasing bow-force limits with increasing β. Both areas are however quite small, indicating that the stability of ALF is critically dependent on the bowing parameters.

In most cases, the string motion could be classified without any problem. However, in the vicinity of the minimum bow force the type of motion could not always be determined unambiguously, due to repeated alternation between Helmholtz motion and multiple slipping. In these cases the classification could depend on where in the 'steady part' the analyzed sample was taken. A restrictive strategy was used by classifying the string motion as Helmholtz motion only when there was no doubt about the stability. Also close to the maximum bow force the detection of Helmholtz motion could be ambiguous due to a large amount of ripple, jitter and pitch flattening. In these cases the adopted strategy was to classify the string vibration as Helmholtz motion if no clear random slip-to-slip

intervals or indications of other types of motion (ALF, S-motion) were found.

3.3. Fitting of Schelleng's bow-force limits

According to equations (1) and (2), the upper and lower bow-force limits are proportional to $1/\beta$ and $1/\beta^2$, respectively, at constant bow velocity v_B and under the assumption that the friction-coefficient delta ($\mu_s - \mu_d$) is constant. The constants of proportionality can be written as

$$c_{upper} = 2Z_0 v_B / (\mu_s - \mu_d) \qquad (6)$$

and

$$c_{lower} = Z_0^2 v_B / 2R(\mu_s - \mu_d). \qquad (7)$$

The Schelleng limits were fitted in the logarithmic domain using a least-squares method, yielding an estimate of c_{upper} and c_{lower} (see Table I) as well as the 95% confidence bounds. To avoid bias the bow-force limits at each β were set between the observed Helmholtz and non-Helmholtz regions. This was achieved by taking the geometric mean of the adjoining points. The fitted bow-force limits are indicated by solid lines in the Schelleng diagrams in Figure 4.

Given the characteristic impedance Z_0 of 0.25 kg/s the obtained values of c_{upper} can now be used to estimate the value of the friction-coefficient delta $\Delta\mu$ (see Table I). The estimated values of $\Delta\mu$ were close to 0.6 except for the lowest bow velocity. These values, however, are slightly overestimated as string torsion has not been taken into account. Assuming that the torsional impedance of the D string used is about a factor two higher than Z_0 (e.g., Schumacher [4]), the total impedance at the string surface Z_{tot} is about 0.17 kg/s, resulting in an estimation of $\Delta\mu = 0.4$. Commonly, values of $\Delta\mu$ observed in experiments, or used in simulations giving realistic output, range between 0.3-0.8 (e.g. Galluzzo [5], Guettler [15], Lazarus [16], Schumacher [17], and Smith & Woodhouse [18]).

3.4. Slope of the bow-force limits in the Schelleng diagram

At some bow velocities, especially 5 and 10 cm/s, the data in Figure 4 suggest that the slope of the upper bow-force limit was not as steep as predicted by equation (1) under the assumption that the friction-coefficient delta $\Delta\mu$ is constant. An estimation of the deviation in slope from the predicted value of -1 was made by comparing the fitted Schelleng limits with an alternative model, in which the slope was added as a fit parameter. It should be noted that such a model has no physical interpretation presently.

The fitted slope values and the 95% confidence intervals plotted versus bow velocity are shown in Figure 5. It can be clearly seen that the slopes of the upper bow-force limits were significantly less steep than the predicted Schelleng slope (-1), except for 20 cm/s. At the two lowest velocities (5 and 10 cm/s) the slopes were only about -0.5. For the lower bow-force limit the fitted slopes were not significantly different from the predicted slope of -2 at all bow velocities. However, the confidence intervals were relatively large. The data in Figure 5 suggest that the

Table I. Values and estimated standard errors of c_{upper} and c_{lower} defining the upper and lower bow-force limits in the Schelleng diagrams in Figure 4 (monochord, steel D string) The values were obtained by fitting the Schelleng limits (equations 1 and 2) to the observed bow-force limits at different bow velocities v_B. The values of c_{upper} were used to estimate $\Delta\mu$. The standard errors were calculated by dividing the 95% confidence intervals of the fit results by a factor 3.92.

v_B [cm/s]	c_{upper} [mN]	c_{lower} [mN]	$\Delta\mu$
5	66 ± 7	0.43 ± 0.06	0.38
10	86 ± 8	0.47 ± 0.04	0.58
15	125 ± 8	0.38 ± 0.05	0.60
20	166 ± 7	0.38 ± 0.06	0.60
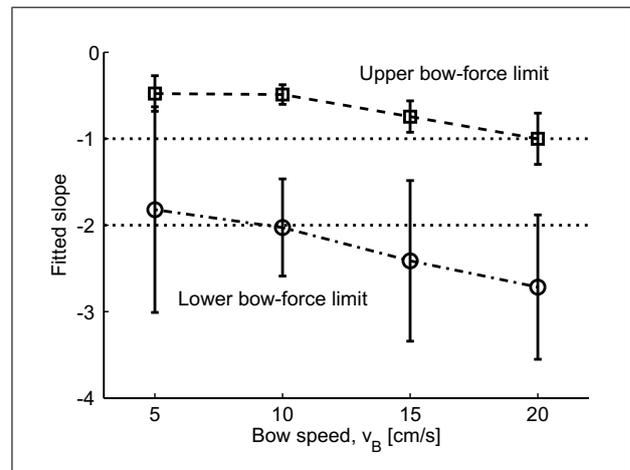
Figure 5. Fitted slopes of the upper bow-force limits (squares, dashed line) and the lower limits (circles, dash-dotted line) in the Schelleng diagrams for different bow velocities in Figure 4. The error bars indicate the 95% confidence intervals of the fitted values. The predicted slopes for maximum and minimum bow force (-1 and -2) are indicated by the horizontal dotted lines.

slopes of both the upper and the lower bow-force limits become increasingly steep with increasing v_B. A possible explanation will be given in the next section.

3.5. Schelleng's bow-force limits based on hyperbolic friction curve

In the preceding fits of the Schelleng limits, $\Delta\mu$ was considered constant. However, as explained in the introduction this is generally not a valid approximation, and the observed deviations in the slope of the upper bow force limit might be explained by variations in $\Delta\mu$. It is therefore likely that the modified Schelleng equations, based on the hyperbolic friction curve (equation 3), would provide a better description of the observed bow-force limits.

For comparison the modified Schelleng equations (4) and (5) were fitted to the observed bow-force limits at different bow speeds. The friction curve parameters were assumed to be $K = 8$ cm/s, $\mu_d' = 0.4$ and $z_0 = 20$ cm/s, based on values commonly used in bowed-string simulations of the violin (e.g., Guettler [15], Woodhouse [19]).

Table II. Values of and estimated standard errors of c'_{upper} and c'_{lower} defining the modified upper and lower bow force limits in the Schelleng diagrams in Figure 4 (monochord, steel D string). The values were obtained by fitting equations (4) and (5) to the observed bow force limits at different bow velocities v_B. The values of c'_{upper} were used to estimate $\Delta\mu'$.

v_B [cm/s]	c'_{upper} [kg/s]	c'_{lower} [g/s]	$\Delta\mu'$
5	1.0 ± 0.24	7.0 ± 1.0	0.51
10	0.73 ± 0.05	4.2 ± 0.4	0.69
15	0.75 ± 0.04	2.3 ± 0.3	0.67
20	0.75 ± 0.03	1.8 ± 0.3	0.67

With these parameters the maximum static friction coefficient becomes $\mu_s = 0.8$ and $(\mu_s - \mu_d) = 0.4$ for $z \to \infty$ (i.e., $\Delta\mu' = 0.4$).

Least-square fits were performed using the logarithmic values of β and F_B. The fit parameters were

$$c'_{upper} = 2Z_0/(\mu_s - \mu'_d),$$

and

$$c'_{lower} = Z_0^2/2R(\mu_s - \mu'_d).$$

In contrast to c_{upper} and c_{lower} (see equations 6 and 7) these fit parameters are independent of bow velocity v_B, and are supposed to be constant. Note that only the choice of z_0 explicitly influences the fitting, as $(\mu_s - \mu'_d)$ is included in the fit parameters.

The fitted upper bow-force limits, corresponding to equation (5) are indicated in Figure 4 with dashed lines. It can be seen that the correspondence with the observed upper bow-force limits was improved in comparison with the earlier fits (solid lines). The differences were more marked at lower bow velocities and explain partly the deviations from the predicted slopes when using the unmodified Schelleng equations as discussed above.

The numerical fit results are displayed in Table II. The values of $\Delta\mu'$ were estimated from c'_{upper}, and were as expected somewhat larger than the estimated values of $\Delta\mu$ in Table I. Taking the lowering by torsion into account the value of $\Delta\mu'$ becomes 0.45.

In Table III the R^2 values of the three alternative fit methods used are shown for all four bow velocities. It can be seen that the straight-line fit with variable slope gave the best fit results. The modified Schelleng equation provided a better fit than the unmodified Schelleng equation, especially at low bow velocities.

3.6. Reproducibility of the Schelleng diagram

In order to assess the reproducibility of the Schelleng diagrams in Figure 4 a comparison was made with a Schelleng diagram measured about five months earlier, using the same experimental setup (string type, bow, monochord), see Figure 6. The bow velocity was 10 cm/s corresponding to Figure 4 (b). The only known difference was that a slightly thinner PVC tape (thickness 0.17 mm) was applied to the string supports. This could have altered the reflection properties somewhat, but this change should not

Table III. R^2 values for the alternative fits of the upper bow-force limits. At bow velocities v_B of 5 and 10 cm/s the R^2 values could not be calculated for the fits of equation (1). In these cases the slope of the observed limits was less steep than -0.5, i.e., a fitted line with slope -1 provided a poorer fit than a horizontal line.

v_B	Basic Sch. (equation 1)	Modified Sch. (equation 5)	Variable slope
5	n/a	0.45	0.75
10	n/a	0.38	0.91
15	0.80	0.85	0.91
20	0.94	0.93	0.94
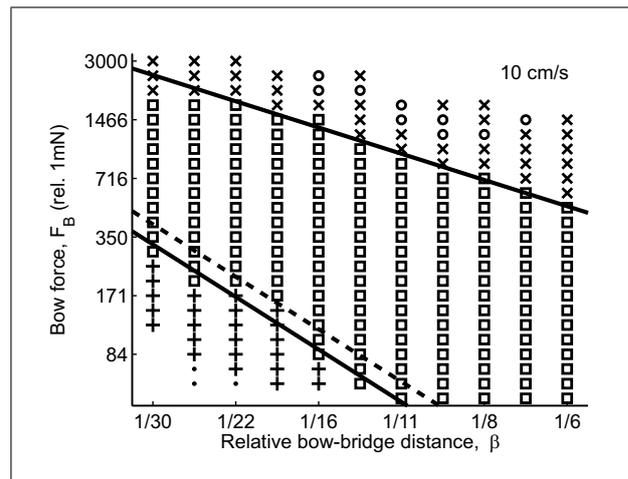
Figure 6. Reproduced Schelleng diagram at a bow velocity of 10 cm/s, measured about 5 months earlier than the corresponding diagram in Figure 4 (b). The solid lines represent the fitted Schelleng limits. The dashed line indicates the fitted lower bow-force limit in Figure 4 (b). The fitted upper bow-force limits coincided exactly.

have a substantial influence (see section 5 for the influence of damping on the bow-force limits).

The fitted bow-force limits (according to equations 1 and 2) are shown in Figure 6 by solid lines. For comparison the fitted bow-force limits of Figure 4 (b) are indicated with dashed lines. It can be seen that the playable regions coincided rather well. The fitted upper bow-force limit coincided exactly with that in Figure 4 (b). Also the region of ALF representing a doubling of the normal fundamental period was found at about the same combinations of bowing parameters.

Some differences could be observed as well. In the Schelleng diagram in Figure 6 the lower bow-force limit was shifted approximately one step down on the force grid, corresponding to about 20%. However, a difference of this magnitude is not unexpected as the determination of the lower force limit always is associated with greater uncertainty than the upper limit (see section 4).

Furthermore, it can be seen that the slope of the fitted upper bow-force limit coincided better with the observed border between Helmholtz and raucous motion than in the unmodified fit in Figure 4 (b). The fitted slope value was

−0.9 compared to −0.5 (see Figure 5) and did not significantly differ from the predicted slope of −1. The cause of this difference is not directly clear but might be related to the amount of rosin or other external conditions mentioned in section 2.5.

All together, the generally good agreement between the two Schelleng diagrams in Figures 4b and 6 indicates that the reproducibility of the measurements was clearly acceptable. It seems safe to conclude that the observed type of string motion was determined by the combination of bowing parameters under control of the bowing machine, and that external conditions only had a secondary influence.

3.7. Schelleng diagrams of the E string

The properties of the strings of the violin vary considerably from the G to the E string. In order to verify the generality of Schelleng's predictions and obtain an estimation of the influence of Z_0 and Z_R Schelleng diagrams were measured for the E string at two bow velocities (10 and 20 cm/s), see Figure 7.

Again, the overall shape of the playable regions with Helmholtz motion was as expected at both bow velocities. For comparison the fitted bow-force limits of the D string in Figure 4 (b) and (d) are indicated with dashed lines. Both the upper and lower bow-force limits of the E string were found to be lower than those of the D string, the upper bow-force limit by 19% and the lower bow-force limit by 64% (at $v_B = 10$ cm/s).

According to equation (1) the upper bow-force limit should be proportional to Z_0 under the assumption that $\Delta\mu$ is similar for both strings. This was clearly not the case, as Z_0 of the E string (0.18 kg/s) was 28% lower than that of the D string. Taking torsion into account explains the difference. Measurements by Schumacher [4] indicate that the ratio Z_R/Z_0 for D strings (gut or synthetic core) is about 2 (1.4-2.4) compared to approximately 3.5 for solid steel E strings (theoretical value 3.7, Cremer [8]). Including torsion in the calculation, the upper limit of the E string is expected to be 16% lower than that of the D string, which is close to the observed 19%. This agreement suggests that $\Delta\mu$ is rather similar for the two strings.

The observed shift of the lower bow-force limit from the D to the E string was larger than the predicted ratio in Z_0^2 given by equation 2 (−48% compared to the observed −64%). Including torsion gave an even poorer agreement (−40%). The discrepancy could probably be attributed to the lower damping of the E string (larger R), as will be discussed in section 5.

3.8. Dependence of bow-force limits on bow velocity

According to equations (1) and (2) both the maximum and minimum bow force, and thus the values of c_{upper} and c_{lower}, should be proportional to v_B. In Figure 8 the experimental data for the bow-force limits for the D and E strings are summarized, showing the estimated values of c_{upper} and c_{lower} versus v_B.
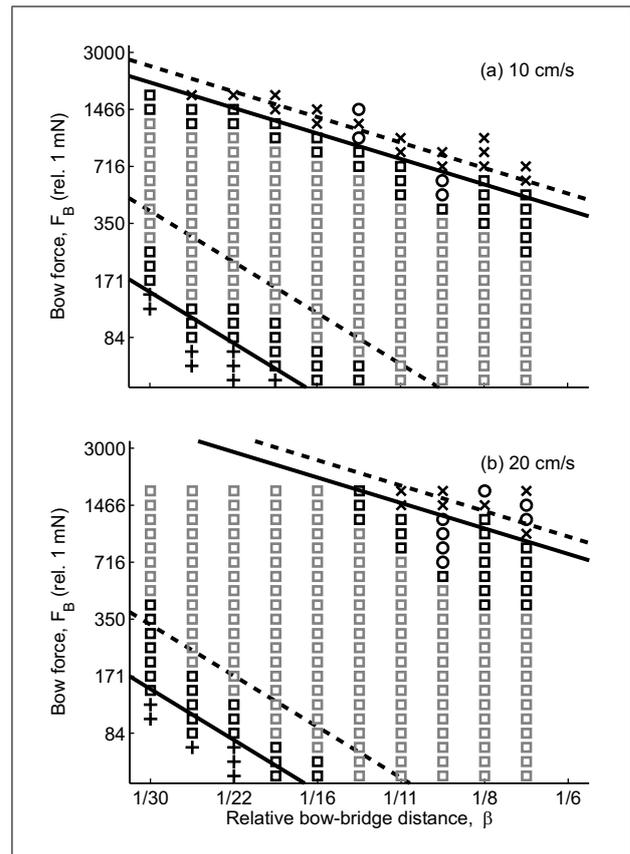
Figure 7. Schelleng diagrams for a steel E string mounted on a monochord at bow velocities (a) 10 and (b) 20 cm/s. The fitted Schelleng limits are indicated with solid lines. The fitted bow-force limits of the D string in Figure 4 are indicated with dashed lines. The middle parts of the Helmholtz regions, indicated by gray squares, were not systematically analyzed, but there was no doubt about the consistency of Helmholtz motion.

For higher bow velocities the upper bow-force limit of the D string was found to be proportional to bow velocity, as can be seen in Figure 8a. The fitted line, which was forced to go through the origin (constant $\Delta\mu$) coincided well with the data, except at 5 cm/s, for which the limit was found to be higher. Also for the E string the upper bow force limit showed proportionality to v_B.

In contrast, the lower bow-force limits for both the D and the E strings showed no clear dependence on bow velocity, as can be seen in Figure 8 (b). Instead, the lower bow-force limits were found to be approximately constant within the measured range of bow velocities, which is in clear contradiction with Schelleng's prediction (equation 2).

4. Experiment II: Minimum bow-force limit – a closer look

An additional experiment was conducted to gain more insight in the transition region around the minimum bow force and the dependence of minimum bow force on bow velocity. One concern regarding Experiment I was that the
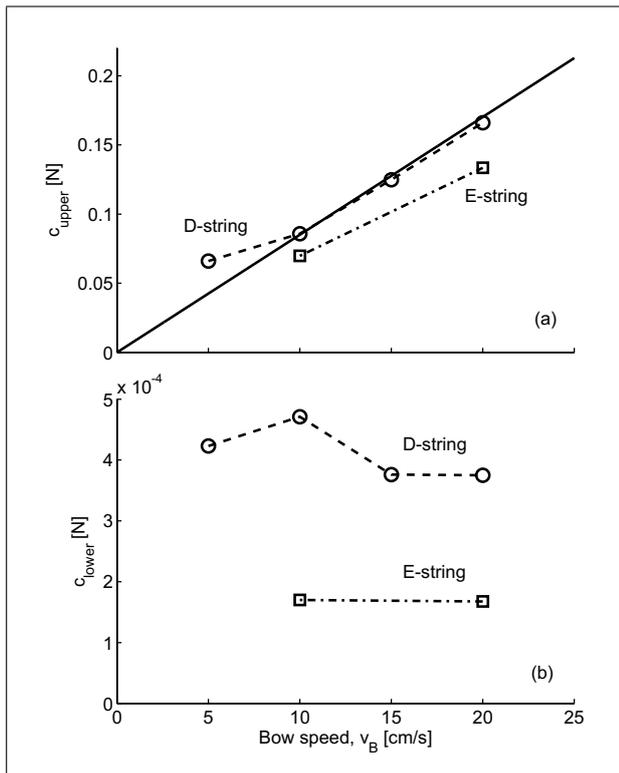
Figure 8. Dependence of the bow-force limits on bow velocity in Experiment I. The plots show (a) c_{upper} and (b) c_{lower} as function of bow velocity, estimated from the Schelleng diagrams of the D string (circles) and E string (squares). According to the Schelleng equations there should be a linear relationship. The solid line in (a) shows a least-squares fit of the upper bow-force limit of the D string according to equation (1), under the assumption that $\Delta\mu$ is constant.

Schelleng diagrams were measured at different occasions over a period of several weeks. For this reason it could not be ruled out with certainty that the results were influenced by changes in experimental conditions. Another problem was that there was some ambiguity in the classification of string motion in the vicinity of the lower bow-force limit due to the occurrence of long transients and mixed types of motion. As the string motion classification was based on a single manually selected interval for each combination of bowing parameters the transition region might not have been characterized correctly, and the possibility exists that the results could somehow have been biased. In the design of the new experiment three main objectives were: (1) to restrict the influence of the external conditions out of the control of the experimenter, (2) to resolve the ambiguity in string motion classification in the vicinity of the lower bow-force limit, and (3) to reduce the significance of the role of the experimenter in the string motion classification procedure.

In Experiment II transitions from Helmholtz to multiple slipping motion were also studied in detail by using bow strokes with a gradually decreasing bow force. The hypothesis was that observations of the changes in string velocity waveforms in the vicinity of the breakdown of

Table IV. Results of string motion classification in Experiment II at $\beta = 1/25$. For each combination of bow velocity v_B and bow force F_B the number of occurrences of Helmholtz motion is displayed (max. 9). The number of cases in which there was doubt about the classification of Helmholtz motion is indicated by a second number. The bold numbers indicate the lower bow-force limit using a heuristic criterion for the definition (see text).

v_B	120	143	171	205	245	293	350	419	501
5	0	0	1/1	3/1	6/1	**9/1**	9	9	9
10	0	0	1/1	0	3	**9**	9	9	9
15	0	0	6/3	7/3	3	**8**	9	9	9
20	0	4/1	9/2	4/1	6/2	6	**8**	9	9

Helmholtz motion could shed some light on the underlying mechanisms.

4.1. Experimental procedure and analysis

The same experimental setup as described earlier was used with the D string on the monochord. The measurements were performed at two β values (1/25 and 1/18 mm) using the same bow velocities as before (5, 10, 15 and 20 cm/s). For each bow-bridge distance a subset of nine bow force values was selected, centered around the minimum bow-force limit found in Experiment I. Each combination of bowing parameters was measured three times. Except for bow-bridge distance, which is not a control parameter of the bowing machine, the measurements were performed in random order (including the three repetitions).

The same string motion classification method as in Experiment I was used with some important modifications of the analysis procedure. For each bow stroke three intervals, each with a duration of 10 nominal periods, were selected for string motion classification. The intervals were taken at predetermined positions within the steady part of the signal. With the three repetitions this provided a total of nine observations for each combination of bowing parameters. The intervals were analyzed in the same random order as they were measured. The bow force value was unknown to the experimenter when performing the classification.

4.2. Determination of lower bow-force limits

The results of the string motion classification are summarized in Tables IV and V. For each bowing parameter combination (β, v_B and F_B) the number of occurrences of Helmholtz motion are displayed (max. 9). All cases of non-Helmholtz motion were found to be multiple slipping motion.

In some cases the string motion was classified as Helmholtz motion by the classification algorithm, but manual inspection of the waveforms gave reason to doubt this judgment. These cases are indicated by a second number in Tables IV and V. In most of these cases the envelopes showed slow fluctuations. Also the slip velocity was much lower than expected for Helmholtz motion. Some examples are shown in Figure 9. In Figure 9a it can be seen

Table V. Results of string motion classification in Experiment II at $\beta = 1/18.1$ (see Table IV for explanations).

v_B	70	84	100	120	143	171	205	245	293
5	2/2	6/1	**9/1**	8	9	9	9	9	9
10	2/1	8/1	**9/1**	9	9	9	9	9	9
15	7/1	**8**	9	9	9	9	9	9	9
20	9/2	**9**	9	9	9	9	9	9	9

that the slip phase became broader as the slip velocity decreased. Closer inspection revealed that the slip phase actually was composed of two slip phases. This is clearer in Figure 9b, where an additional slip phase can be distinguished as it grows into the main slip. At the same time the amplitude of the main slip decreases. Other examples are shown in Figure 9c and d. In the last example it can be clearly seen that there is a double slip phase. The behavior of the string motion is not completely clear in these cases and seems to represent some kind of long-lasting transient behavior (further discussed in section 4.4). For this reason string motions displaying this type of behavior were not considered as pure Helmholtz motion.

The minimum bow force was determined for the eight combinations of β and v_B, using a heuristic criterion. The lowest bow force at which at least eight out of the nine selected intervals were undoubtedly classified as stable Helmholtz motion was taken as the minimum bow-force limit. These values, which imposes a rather strict criterion on Helmholtz motion at the lower limit, are indicated in Tables IV and V in bold. The obtained values were close to the lower bow-force limits observed in Experiment I (see Figure 4). It was noted, however, that the values for $\beta = 1/18$ (Table V) were consistently lower than those in Figure 4 by 2-4 grid steps, suggesting a somewhat steeper slope for the lower bow-force limit than found in Experiment I.

4.3. Dependence on bow velocity

The values of c_{lower} at each bow velocity were calculated by multiplying the found values of minimum bow force in Tables IV and V with β^2 and taking the geometric average across β. This way of calculating c_{lower} is identical to fitting a straight line with slope -2 in the log-log representation of bow force versus β.

In Figure 10 the estimated values of c_{lower} are plotted as function of v_B. The best linear fit together with the 95% prediction bounds are shown as well. The figure clearly shows that the slope was not significantly different from zero, which indicates that there was no dependence of the lower bow-force limit on bow velocity. The results of Experiment II thus confirm the observations in Experiment I. In contrast to Schelleng's predictions, the experiments show that the lower bow-force limit was independent of bow velocity in the measured range 5-20 cm/s. It can be noted that bow velocities around 20 cm/s are typical in normal violin playing (Askenfelt [2]).
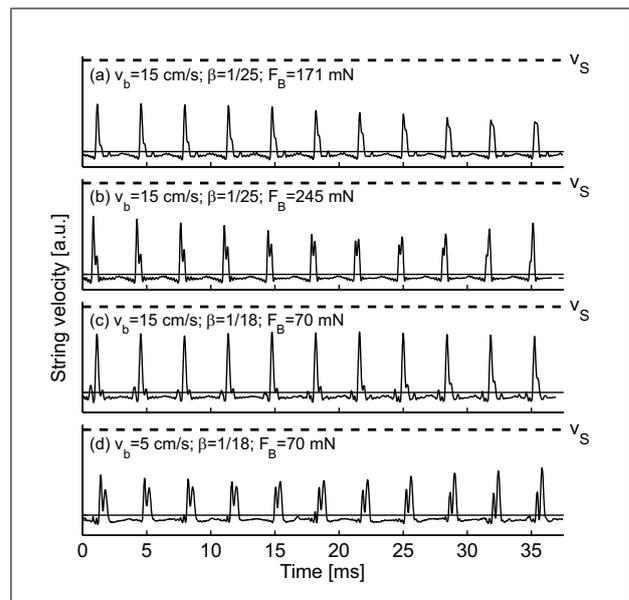
Figure 9. Examples of string velocity waveforms in the vicinity of the minimum bow force (D string). In all examples only one slip phase per fundamental period was detected, but closer inspection revealed the presence of an additional slip phase included in the main slip, leading to a prolonged slip phase. It was also observed that the maximum slip velocity was significantly lower than the nominal slip velocity for Helmholtz motion v_S (indicated at the top of the panels by dashed lines). The slow fluctuations in the waveform indicate transient behavior, even after one or more seconds of steady bowing.
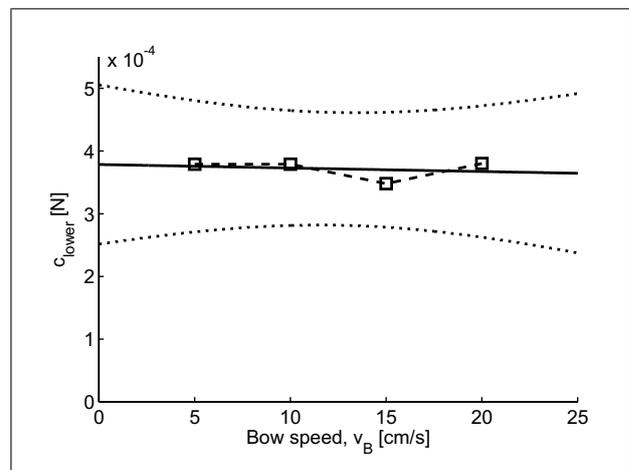
Figure 10. Mean values of c_{lower} versus bow velocity for the D string in Experiment II. The best linear fit (solid line) and the 95% prediction interval (dotted lines) indicate that the minimum bow-force limit was not dependent on bow velocity within the measured range 5-20 cm/s.

4.4. Breakdown of Helmholtz motion at minimum bow force

In order to gain more insight in the breakdown of Helmholtz motion at minimum bow force, measurements were made using bow strokes with gradually decreasing force. The bowing parameter profiles were similar to the ones de-
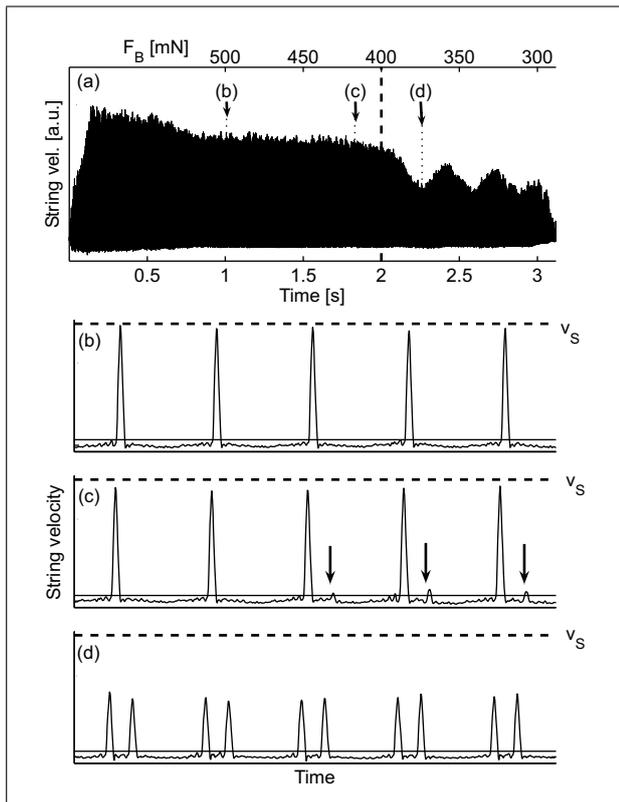
Figure 11. Breakdown of Helmholtz motion at minimum bow force (D string). The string velocity signal shown in (a) resulted from a bow stroke with a slowly linearly decreasing bow force F_B (the decreasing bow force during the semi-steady part of the bow stroke is indicated in (a) by the upper axis). The relative bow-bridge distance β was 1/21.7. The transition from Helmholtz to non-Helmholtz motion is marked with a vertical dashed line. After the transition the string motion became unstable as can be seen from the envelope, including two slip phases which grow and diminish alternately. The envelope shows a minimum when both slip phases are equal in magnitude. Selected parts of the signal, indicated by the arrows in (a), are shown in close-up in (b), (c) and (d). The nominal slip velocity v_S is indicated by the horizontal dashed lines (v_B was calculated from the uncalibrated string velocity signal by taking the median of selected stick phases of the signal in the time interval 0.85-1.75 s; v_S was calculated as $v_B(\beta - 1)/\beta$.

scribed in section 2.4, except that the constant bow force during the steady phase T_{steady} was replaced with a slowly linearly decreasing bow force. The initial force and the gradient were chosen so that the string was in Helmholtz motion in the beginning of the 'decreasing' (semi-steady) phase and the minimum bow force was passed about in the middle of this phase.

A typical transition from Helmholtz motion to multiple slipping is shown in Figure 11. It can be clearly seen from the envelope in panel (a) that the string motion becomes unstable after the transition (marked by the dashed line). Selected parts of the string velocity waveform are shown in panels (b) to (d). The estimated values of the velocity during stick v_B and the slip velocity v_S are also indicated, showing the outline of ideal Helmholtz motion.
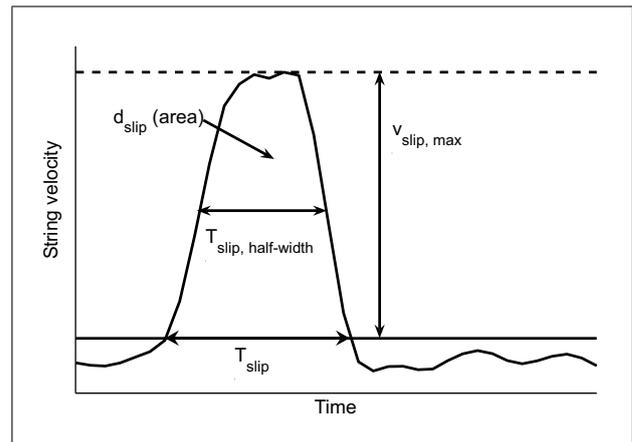
Figure 12. Features used to characterize the shape of the slip phase: the traversed distance during slip (area of the slip phase, d_{slip}), the maximum slip velocity $v_{slip,max}$, the duration of the slip phase T_{slip} and the width of the slip phase at half height $T_{slip,half-width}$.

Before the transition Helmholtz motion was observed as can be seen in panel (b), with stick and slip velocities corresponding to ideal Helmholtz motion. Just before the transition (panel c) the nominal slip velocity v_S was no longer reached. Furthermore, the string motion became more agitated during the stick phase and a tendency to form extra slips could be observed (indicated by the arrows). It could be noted that the secondary slip appears quite early after the main slip, and not in the middle of the stick phase as predicted by the Raman/Schelleng model. Simulations indicate that the explanation is related to ripple in friction force (see section 6.3).

At the transition an additional slip was finally formed and started to grow, while the main slip diminished. At $t \approx$ 2.3 s (panel d) the second slip became larger than the main slip, which finally disappeared completely. Just before the 'old' main slip disappeared (at $t \approx 2.6$ s) another small slip was formed just after the 'new' main slip, and the process repeated itself.

For studying the effect of corner rounding on the shape of the slip phase the following features were determined as indicated in Figure 12: the area of the slip phase (traversed distance) d_{slip}, the maximum slip velocity $v_{slip,max}$, the duration of the slip phase T_{slip}, and the width of the slip phase at half-height $T_{slip,half-width}$. The latter measure could be considered as the effective width of the slip phase, mostly dependent on the position on the string where the string velocity was measured and to a lesser degree on corner rounding.

Figure 13 shows the continuous change in the features of the slip shape of the signal shown in Figure 11. The maximum slip velocity $v_{slip,max}$ decreased with decreasing bow force when the string was in Helmholtz motion ($t = 1$-2 s). At the same time the slip duration T_{slip} increased. Consequently, the displacement during the slip phase d_{slip} remained relatively constant, close to its nominal value until shortly before the transition. These changes
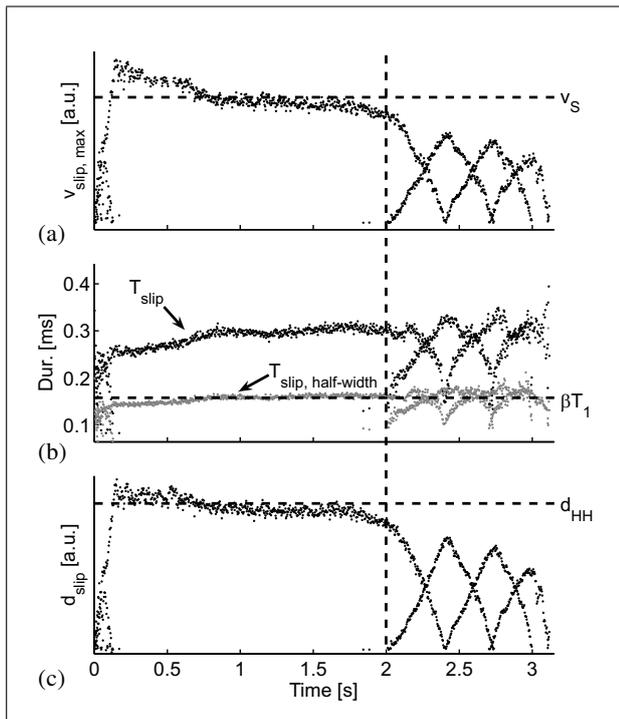
Figure 13. Development of the slip shape during a bow stroke with decreasing bow force extracted from the string velocity signal shown in Figure 11: (a) Maximum slip velocity ($v_{slip,max}$), (b) the two width features (T_{slip} and $T_{slip,half-width}$), and (c) the distance traversed during slip phase (d_{slip}). The minimum bow-force limit is reached at the vertical dashed line. The nominal values of the slip speed v_S, slip duration βT_1 and displacement $v_B T_1(\beta - 1)$ for ideal Helmholtz motion are indicated by horizontal dashed lines.

could be attributed to the increasing effect of corner rounding with decreasing bow force. After $t \approx 1.8$ s the slip phase started to collapse, as can be seen from the pronounced decrease in v_{slip} and d_{slip}, marking the beginning of the breakdown of Helmholtz motion. Immediately after the transition the presence of an additional slip phase which successively grows in prominence is clearly visible in all panels. Also the process of mutual growing and diminishing of the co-existing slip phases is clearly visible. Even after the transition, the shape of the slip phase continued to change due to the increasing effect of corner rounding. For example at $t = 2.4$ s, the point at which the original slip phase had disappeared almost completely, the dominant slip phase was broader (T_{slip}) and its maximum slip velocity $v_{slip,max}$ was lower compared to the single slip phase just before the transition.

5. Experiment III: The role of damping

In deriving the expressions for the bow-force limits, Schelleng used the Raman string model, in which one string termination is fixed and the other represented by a mechanical resistance R. As pointed out by Schelleng R may be thought of as composed of two components in parallel, one being the resistance of the body of the instrument and the other representing the combined losses due to (a) internal

friction of the string, (b) the losses at the contact point with the bow, and (c) the losses due to the reflection at the upper end of the string (finger/nut).

As R appears in the Schelleng equation for the minimum bow force (equation 2) it is desirable to determine its value by experiments. This would shed light on the influence of the instrument, the string, and the stopping of the string with the finger. Furthermore, by estimating R, the empirically found lower bow-force limits could be directly compared with the theoretical value from Schelleng equation (2).

For this purpose, additional measurements were performed using an identical D string as in Experiment I and II on a violin. The bow-force limits were obtained both for open and stopped strings. The string was stopped by clamping a piece of expanded polystyrene against the string. The damping, which could be modified by changing the pressure of the clamp was adjusted to be similar to the damping of a finger in normal playing conditions by comparing the decay times of pizzicato notes.

5.1. Determination of Q values and the mechanical resistance R

The mechanical resistance R with the string mounted on the monochord and the violin, respectively, were determined from plucked-string signals. The plucking was performed by pulling the string in the bowing direction with a loop of a thin copper wire until it broke. The relative plucking point β was about 1/18.

The Q value of the fundamental string mode for different conditions (instrument, string, open/stopped) was determined from the decay time τ_1 of the fundamental

$$Q_1 = \pi f_1 \tau_1.$$

where f_1 is the fundamental frequency. The mechanical resistance R was calculated as (see Appendix)

$$R \approx 2Z_0 f_1 \tau_1.$$

The values of τ_1, Q_1 and R (averaged across 2-4 plucks) are displayed in Table VI for four string-instrument combinations. The Q_1 values of the open D strings on the monochord and the violin, respectively, were rather similar (480 and 410). This is about a factor two lower than the values measured on a rigid test bench (Jansson [20]). The agreement between the Q values for the monochord and violin indicates that the tape on the bridge and the plastic nut introduced suitable losses for the lowest mode in order for the monochord to behave 'violin-like.' When stopping the string Q_1 was significantly decreased to 281 (−40%). Q_1 for the open E string on the monochord was about a factor two greater than for the D string. This is most likely due to lower internal losses in the solid E string compared to the wound D string.

Table VI. Damping characteristics for four string-instrument combinations. The measured decay time of the fundamental τ_1 in plucked-string signals was used to calculate Q_1 and R. The estimated errors are based on the standard deviation of τ_1. For the stopped D string on the violin only one pluck was measured.

Instrument, string	Z_0 [kg/s]	τ_1 [s]	Q_1	R [kg/s]
Monochord, D	0.25	0.521 ± 0.016	480 ± 14	76 ± 2.3
Violin, D (open)	0.25	0.448 ± 0.017	410 ± 15	65 ± 2.5
Violin, D (stopped)	0.25	0.296	281	45
Monochord, E	0.18	0.457 ± 0.004	945 ± 8	108 ± 1.0

5.2. Dependence of bow-force limits on damping

The same method as in section 4.4 with gradually increasing or decreasing bow force was used to determine c_{upper} and c_{lower} for different damping conditions. The force at which breakdown of Helmholtz motion was observed was taken as the force limit. This was done for 3-4 bow-bridge distances (depending on the range in which the transition could be observed) with two or three repetitions. The values of c_{upper} and c_{lower} were obtained by multiplying the found maximum and minimum bow forces with β and β^2, respectively, and taking the geometric mean. The values of $\Delta\mu$ were again obtained from the found values of c_{upper}, using equation (6). The values of c_{lower} according to Schelleng were calculated from equation (7), using the estimated values of $\Delta\mu$ and R in Table VI.

In Table VII the empirically determined values of c_{upper} and c_{lower} for the monochord and violin (open and stopped string) are summarized. Comparing the three conditions for the D string it can be seen that the upper bow-force limit was not completely independent of damping as predicted by Schelleng. A tendency to increase with decreasing R was observed. As R dropped to 60% from monochord to stopped string condition, the upper limit increased by 20%.

In contrast, the minimum bow force showed a strong dependence on R. The observed lower bow-force limit was a factor 1.5 higher for the open D string on the violin compared with the monochord, and increased significantly to a factor 3.4 when stopping the string. The dependence on R was thus much stronger than the inverse proportionality predicted by equation ((2)). For the three damping cases measured with the D string the dependence was well described by $c_{lower} \propto R^{-2.3}$.

Comparing the magnitude of the empirically found values of c_{lower} with the values estimated using equation (7), it can be seen that Schelleng's equation provided a gross underestimation of the minimum bow force for all cases. The empirically found lower bow-force limits were almost one order of magnitude larger (a factor 6-11). It is not plausible that this discrepancy could be attributed to errors in the determination of the damping characteristics alone, which gave reasonable values. The results mean that in all cases the observed playable force ratio F_{max}/F_{min} was much smaller than the theoretical value of $4R\beta/Z_0$.

In section 3.7 it was observed that the measured lower bow-force limits of the D and E strings differed more than predicted by the change in Z_0^2. Taking the different values of R of the D and the E string into account (76 and 108 kg/s) the Z_0^2/R ratio becomes 0.36, which coincides exactly with the observed -64% shift of the lower limit. Taking torsion into account the predicted decrease amounts 57%, which is slightly less in agreement with the observed shift.

6. Discussion

6.1. Empirical Schelleng diagrams

In the experiments a number of aspects of Schelleng's predictions of upper and lower limits of bow force have been examined. Generally, a rather good agreement between theory and observations was found. Most discrepancies were encountered in the determination of the lower bow-force limit, in particular the dependence on bow velocity. In contrast to Schelleng's predictions the lower limit was found to be independent of bow velocity, and a follow-up experiment was run to verify the results. Some methodological issues are of particular interest to consider.

The experiments gave a clear indication of the fact that there are some principal difficulties in the classification of the string motion in the vicinity of the minimum bow force. As shown in section 4 there is a gray zone between clear cases of Helmholtz motion and multiple slipping, characterized by an alternation between these two types of motion, compound slip phases (composed of two neighboring slip phases), and long transients. This means that the determination of the minimum bow force will always be dependent on criteria set by the experimenter, either in manual judgments of individual cases, or coded in an automatic classification algorithm. In this study a combination of manual judgment guided by an interactive classification algorithm was used in order to arrive at highest possible confidence in the classification. Each decision was based on data on the string waveform compiled by a classification algorithm into a 'decision chart' which gave characteristic patterns for the different types of string motion. Influence of the experimenter's prejudices was reduced as far as possible by hiding information about the combination of bowing parameter values. In this way consistency in the judgments was assured at the same time as each classification was checked for being reasonable.

The performance of the bowing machine and the influence on the string motion is an essential aspect. As described in section 2 there were some fluctuations in bow force during a bow stroke. Accurate control of bow force

Table VII. Bow-force limits and estimated standard errors for the four string-instrument combinations in Table VI at $v_B = 10$ cm/s. The predicted values of c_{lower} according to Schelleng, calculated using equation (7), and the estimated values of R and $\Delta\mu$ are displayed in the last column.

Instrument, string	R [kg/s]	c_{upper} [mN]	$\Delta\mu$	c_{lower} [mN]	$c_{lower, Schelleng}$ [mN]
Monochord, D	76	86 ± 8	0.58	0.47 ± 0.04	0.070
Violin, D (open)	65	91 ± 8	0.55	0.69 ± 0.04	0.088
Violin, D (stopped)	45	103 ± 2.4	0.49	1.56 ± 0.13	0.143
Monochord, E	108	70 ± 2.3	0.52	0.17 ± 0.02	0.029

is a difficult problem due to the combination of relatively heavy bow and low bouncing frequency against the string. The relative amplitude of the fluctuations was rather large at low forces, and at the lowest target force (49 mN) the relative RMS fluctuation reached 20-30%. However, the relative error decreased rapidly with increasing bow force and for a majority of the measurements (85% with target values above 100 mN) the fluctuations were well below 10%. For comparison, Galluzzo [5] using a more complex control strategy and more powerful bowing machine to play a cello bow reported a maximum fluctuation error in bow force of 3%. However, these values cannot be directly compared as Galluzzo measured Guettler diagrams with accelerating bow at higher bow forces (min. 0.5 N).

The effect of the fluctuations, which would have the largest influence on the determination of the lower bow force limit, is not exactly known. It could be speculated whether the surprising result that the lower bow force limit was independent of bow velocity is related to unsatisfactory control of bow force. Admittedly, it is possible that the pattern of Helmholtz motion could be disturbed by fluctuations in force when approaching the lower limit, which in turn would lead to an overestimation of the minimum bow force. Such an effect would be particularly evident for the lowest forces at large β values. The measurements showed, however, no indications of this type of artifact. The data indicate a linear slope of about $1/\beta^2$ for the lower limit throughout the β range, without a noticeable upward curvature in the low forces at large β values. Furthermore, clear differences in the levels of minimum bow force could be observed between the D and E strings, both showing the expected slope of about $1/\beta^2$. All together these observations indicate that the control of bow force was accurate enough for the purposes of the current study. In particular, it can be concluded that bow-velocity dependent changes in the lower bow-force limit should have been observed if there were any.

6.2. Maximum bow force

The upper bow-force limits determined in this study are in good agreement with measurements of Schumacher [4], who reported values of c_{upper} for a number of violin D strings of different types in the range of 75-109 mN at $v_B = 10$ cm/s on a violin (cf. 91 mN in the current study).[2]

---

[2] The maximum bow forces reported by Schumacher were expressed in normalized units. The values of c_{upper} were calculated from equation (5) in [4]

For the two plain steel E strings in his study, he found maximum bow forces corresponding to values of c_{upper} of 88 and 98 mN. These values are somewhat higher than the value of $c_{upper} = 70$ mN (monochord) in the current study.

For the determination of $\Delta\mu$ it is important to take torsion into account. The change is proportional to the ratio Z_{tot}/Z_0, which lowered the estimated values for the D and E string about 30% and 20%, respectively.

An interesting observation was that the slope of the upper bow-force limit in the Schelleng diagram increased with increasing bow velocity, approaching the theoretical value of -1. This could be attributed to a variation in the friction coefficient delta $\Delta\mu$ with bow velocity by fitting the modified Schelleng equation (based on a hyperbolic friction curve) to the data. This functional behavior of $\Delta\mu$ gave a better fit than the assumption of a constant $\Delta\mu$, indicating that the variation in $\Delta\mu$ with bow velocity is clearly reflected in the empirical Schelleng diagrams.

6.3. Minimum bow force

Regarding the minimum bow force the experiments showed some marked deviations from Schelleng's theoretical description. Firstly, there was no significant dependence of minimum bow force on bow velocity within the measured range of bow velocities (5–20 cm/s). Secondly, it was shown in section 5 that the dependence of the minimum bow force on damping (represented by the estimated value of R) was much stronger than inversely proportional. Furthermore, it was shown that Schelleng's equation for minimum bow force (2) lead to a gross underestimation of the lower bow-force limit, using the estimated values of R.

All together, these observations put the mechanism causing breakdown of Helmholtz motion at minimum bow force proposed by Schelleng severely into question. The Schelleng equations are based on the assumption that the impedance of the bridge termination is purely resistive, which means that corner rounding and ripple are ignored. However, as suggested by Woodhouse [3] ripple might be an important source of perturbation for the breakdown of Helmholtz motion. This can also be seen in Figure 11 (c), which shows the 'seeds' of an additional slip phase.

In Raman's analysis the reflection functions are of the Dirac-delta type (giving Q values proportional to the harmonic numbers). One useful feature here is a friction force rising in steps from a minimum value equal to $F_B\mu_d$ during the slip interval to a maximum occurring somewhere
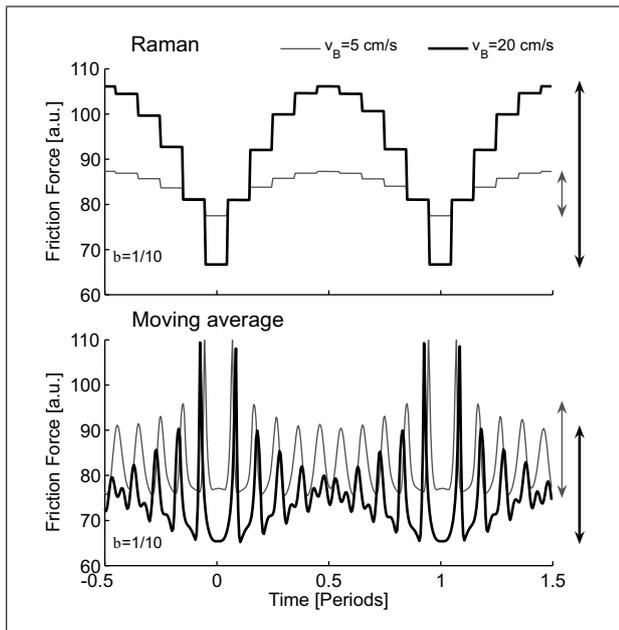
Figure 14. Periodically repeating patterns of friction force simulated with hyperbolic friction model (not including torsion and dispersion). The upper panel shows the patterns resulting from the Raman model, on which Schelleng based his calculations. There is a proportionality between bow velocity (v_B) and the force range which determines the minimum bow force. The lower panel shows the pattern resulting from the same bowing parameters applied to a model with narrow reflection functions (Q-values fading with increasing frequency). The slipping intervals vary in length. The resulting ripple force range (excluding transitional spikes) at $v_B = 20$ cm/s is a mere 17% wider than at 5 cm/s, as opposed to 300% with the Raman model. The range of periodic friction-force variation is indicated by the double arrows.

close to the middle of the stick interval, when the string is excited at an integer-ratio position. Raman showed this periodic change of friction to be proportional to bow velocity. However, with any kind of slightly more realistic damping, the step-like force buildup would be replaced by a force ripple, with maxima most likely to occur at the instance βT_1 before the stick-slip transition (caused by reflections from the nut), or βT_1 after the slip-stick transition (caused by reflections from the bridge). Simulations show that these are due to rounded-corner sharpening ('echos'), a feature not present in the Raman model. The ripple amplitudes are dependent (although not linearly) on the length of the slip interval, friction-coefficient delta, and damping properties, but are not directly related to bow velocity. At minimum bow force a certain degree of subharmonic interference [21] often contributes to further blurriness. It is thus hard to see how the Raman model could be useful for estimation of minimum bow force.

Figure 14 shows the effect of Raman damping versus a moving-average type of damping. The range of periodic friction-force variation, equal to $F_B(\mu_s - \mu_d)$, determines the minimum bow force in all cases. A clear difference in the behavior of these damping models with respect to

bow velocity can be observed. As opposed to the Raman model (upper panel), which shows a proportional relation between minimum bow force and bow velocity, the model with narrow reflection functions shows a mere 17% increase of minimum bow force when bow velocity is increased from 5 to 20 cm/s. More generally, simulations showed that the influence of bow velocity on minimum bow force is dramatically reduced for large values of β, and shows only limited effects (never proportionally) at smaller β. Since both the empirical results and simulations suggest that Schelleng's calculations for minimum bow force might be based on faulty assumptions, these issues are certainly worth further investigation.

Closing the discussion of the lower limit of bow force it can be speculated about the significance for the player. From the performer's point of view the lower limit in bow force may not be as critical as the upper. A low bow force in the vicinity of the lower limit is typically used for *pp* playing at relatively large values of β. For such cases a certain amount of multiple slipping in the waveform is not easily perceptible, particularly not in orchestral playing. In contrast, the player needs to have a good feeling for the margins to the upper bow force limit when exploring the *ff* range, notably for long notes played with a low bow velocity. Here, the amount of pitch flattening and noise content are helpful by giving continuous indications of how far away the disastrous switch-over to raucous motion actually is.

7. Conclusions

In this study bow-force limits for bowed violin strings were systematically measured for wide ranges in bow-bridge distance and bow force, covering a substantial part of the ranges used in normal violin playing (β values 1/30-1/6, bow forces 49-3000 mN). In the measurements a normal violin bow was used to play a monochord and a violin. The bow velocity and the bow force were controlled by a bowing machine. The results were compiled in empirical Schelleng diagrams for four bow velocities (5, 10, 15, 20 cm/s).

Summarizing the results, it was found that there was generally a good qualitative agreement between the empirical Schelleng diagrams and the properties predicted by Schelleng. There was a continuous playable region in the central part with Helmholtz motion ('Schelleng's triangle'), surrounded by regions of raucous motion and anomalous low frequencies (ALF) at higher bow forces and multiple slipping at lower forces.

The upper and lower bow-force limits for Helmholtz motion formed approximately straight lines in the log-log Schelleng diagrams. The slope of fitted upper limits was found to be less steep than the predicted value of −1, in particular for low bow velocities. A better agreement with measurements was reached by taking the variation in friction-coefficient delta with bow velocity into account. This was done by incorporating a hyperbolic friction curve in the model (modified form of Schelleng's equation). The

magnitude of the upper bow force was proportional to bow velocity in accordance with predictions. Damping at the string terminations influenced the upper limit to some extent, which is not in line with Schelleng's predictions.

The lower bow-force limit showed no significant deviation from the predicted slope of -2. However, three other results did not correspond with predictions at all: (1) the lower limit was not dependent on bow velocity, (2) the magnitude of the lower bow force was an order of magnitude higher than predictions, and (3) the dependence of damping was far stronger than inversely proportional. These findings suggest that Schelleng's derivation of the lower limit for Helmholtz motion was not based on correct assumptions, a conclusion confirmed by simulations with different types of reflection functions.

The experiments showed that the transition from Helmholtz motion to multiple slipping at the lower limit is not well defined but covers a gray zone in which the classification of string motion is ambiguous. Observations show that as bow force is reduced the slip phase becomes distorted and additional small slips start to grow and replace the main slip in a repeated pattern before complete breakdown of Helmholtz motion occurs. Simulations indicate that the mechanisms involved include effects of corner rounding and resharpening at release which give rise to substantial ripples in friction force. The magnitude of these ripples is not reduced in proportion to bow velocity. Such effects were not taken into account by Schelleng, who based his derivation on the well-behaved friction force in the Raman model. This model predicts a periodic variation in force with a magnitude directly proportional to bow velocity.

Appendix

Calculation of the mechanical resistance R

The formula for calculating the mechanical resistance R from the decay time τ_1 of the fundamental string mode according to Raman's string model can be derived as follows.

The reflection factor of the bridge termination of the string is given by

$$\lambda = \frac{Z_0 - R}{Z_0 + R}, \tag{A1}$$

where Z_0 is the characteristic wave impedance (cf. [8], equation 5.21). The relative amount of reflected energy per fundamental period T_1 (one lossy reflection) is

$$|\lambda|^2 = e^{-2T_1/\tau},$$

where τ the decay time, so that

$$\tau = \frac{T_1}{\ln(1/|\lambda|)}. \tag{A2}$$

According to the Raman model the decay times of all string modes are equal, which is not in agreement with observations of real strings. For the calculation of R only

the fundamental is considered as it dominates the decay. For a quasi-fixed termination ($R > Z_0$) the combination of equations (A1) and (A2) yields

$$R = Z_0 \frac{e^{T_1/\tau_1} + 1}{e^{T_1/\tau_1} - 1},$$

which can be written as

$$R = Z_0 \coth(T_1/2\tau_1).$$

For small arguments ($\tau_1 \gg T_1$) this can be approximated by

$$R \approx \frac{2Z_0\tau_1}{T_1}, \tag{A3}$$

which is identical to [8], equation (4.32a).

Using the relation between Q and τ

$$Q = \pi f \tau,$$

where f is the mode frequency, the Q value can be written as

$$Q = \frac{\pi}{\ln(1/|\lambda|)},$$

and

$$R \approx \frac{2Z_0 Q}{\pi}.$$

For an alternative derivation, see [22], equation (2.45) case (1), for $R \gg Z_0$.[3]

References

[1] J. C. Schelleng: The bowed string and the player. J. Acoust. Soc. Am. **53** (1973) 26–41.

[2] A. Askenfelt: Measurement of the bowing parameters in violin playing. II: Bow-bridge distance, dynamic range, and limits of bow force. J. Acoust. Soc. Am. **86** (August 1989) 503–516. Reprinted in Research paper in violin acoustics 1975-1993, ed. Hutchins, pp. 305-318.

[3] J. Woodhouse: On the playability of violins. Part II: Minimum bow force and transients. Acustica **78** (1993) 137–153. Reprinted in Research paper in violin acoustics 1975-1993, ed. Hutchins, pp. 283-299.

[4] R. T. Schumacher: Measurement of some parameters of bowing. J. Acoust. Soc. Am. **96** (1994) 1985–1998. Reprinted in Research paper in violin acoustics 1975-1993, ed. Hutchins, pp. 255-268.

[5] P. M. Galluzzo: On the playability of stringed instruments. Dissertation. Trinity College, University of Cambridge, October 2003.

[6] C. V. Raman: Experiments with mechanically-played violins. Proc. Indian Assoc. Cultivation Sci., 1920-1921, 19–36. Reprinted in Musical Acoustics, Part I, ed. Hutchins, pp. 186-204.

---

[3] Note the misprint in the following paragraph in the third edition of [22] discussing the wave pattern of case (2), referred to as a fixed-fixed string instead of the correct fixed-free string. Case (1) corresponds to the fixed-fixed string.

[7] N. C. Pickering: Physical properties of violin strings. J. Catgut Acoust. Soc. **44** (1985) 6–8. Reprinted in Research paper in violin acoustics 1975-1993, ed. Hutchins, pp. 229-232.

[8] L. Cremer: The physics of the violin. The MIT Press, 1984.

[9] B. Lawergren: Harmonics of S motion on bowed strings. J. Acoust. Soc. Am. **73** (1983) 2174–2179. Reprinted in Research paper in violin acoustics 1975-1993, ed. Hutchins, pp. 177-182.

[10] J. Woodhouse: On the playability of violins. Part I: Reflection functions. Acustica **78** (1993) 125–136. Reprinted in: Research paper in violin acoustics 1975–1993, ed. Hutchins, pp. 271-282.

[11] F. A. Saunders: The mechanical action of violins. J. Acoust. Soc. Am. **9** (1937) 81–98.

[12] X. Boutillon: Analytical investigation of the flattening effect: the reactive power balance rule. J. Acoust. Soc. Am. **90** (1991) 754–763.

[13] A. Cronhjort: A computer-controlled bowing machine (MUMS). STL-QPSR **33** (1992) 61–66.

[14] J. Woodhouse: Bowed string simulation using a thermal friction model. Acustica united with Acta Acustica **89** (2003) 355–368.

[15] K. Guettler: On the creation of the helmholtz motion in bowed strings. Acustica united with Acta Acustica **88** (2002) 970–985.

[16] H. Lazarus: Die Behandlung der selbsterregten Kippschwingungen der gestrichenen Saite mit Hilfe der endlichen Laplacetransformation. Dissertation. Technical University of Berlin, 1972.

[17] R. T. Schumacher: Self-sustained oscillations of the bowed string. Acoustica **43** (1979) 109–120. Reprinted in Research paper in violin acoustics 1975-1993, ed. Hutchins, pp. 243-254.

[18] J. H. Smith, J. Woodhouse: The tribology of rosin. J. Mech. Phys. Solids **48** (2000) 1633–1681.

[19] J. Woodhouse, P. M. Galluzzo: The bowed string as we know it today. Acustica - Acta Acustica **90** (2004) 579–589.

[20] E. Jansson: Acoustics for violin and guitar makers. Dept. of Speech Music and Hearing, Royal Institute of Technology (KTH), 2002.

[21] J. Woodhouse: On the stability of bowed string motion. Acustica **80** (1994) 58–72.

[22] L. E. Kinsler, A. R. Frey, A. B. Coppens, J. V. Sanders: Fundamentals of acoustics. Third ed. John Wiley & Sons, Inc., 1982.